LETTERS
PUBLISHED ONLINE: 2 AUGUST 2009 | DOI: 10.1038/NPHYS1362
nature physics

Evidence for reversible control of magnetization in a ferromagnetic material by means of spin–orbit magnetic field

Alexandr Chernyshov[1]*, Mason Overby[1]*, Xinyu Liu[2], Jacek K. Furdyna[2], Yuli Lyanda-Geller[1] and Leonid P. Rokhinson[1]†

The current state of information technology accentuates the dichotomy between processing and storage of information, with logical operations carried out by charge-based devices and non-volatile memory based on magnetic materials. The main obstacle for a wider use of magnetic materials for information processing is the lack of efficient control of magnetization. Reorientation of magnetic domains is conventionally carried out by non-local external magnetic fields or by externally polarized currents[1–3]. The efficiency of the latter approach is enhanced in materials where ferromagnetism is carrier-mediated[4], because in such materials the control of carrier polarization provides an alternative means for manipulating the orientation of magnetic domains. In some crystalline conductors, the charge current couples to the spins by means of intrinsic spin–orbit interactions, thus generating non-equilibrium electron spin polarization[5–11] tunable by local electric fields. Here, we show that magnetization can be reversibly manipulated by the spin–orbit-induced polarization of carrier spins generated by the injection of unpolarized currents. Specifically, we demonstrate domain rotation and hysteretic switching of magnetization between two orthogonal easy axes in a model ferromagnetic semiconductor.

In crystalline materials with inversion asymmetry, intrinsic spin–orbit interactions couple the electron spin with its momentum $\hbar\mathbf{k}$. The coupling is given by the Hamiltonian $\mathcal{H}_{so} = (\hbar/2)\hat{\sigma}\cdot\mathbf{\Omega}(\mathbf{k})$, where $\hbar$ is the reduced Planck constant and $\hat{\sigma}$ is the electron spin operator (for holes $\hat{\sigma}$ should be replaced by the total angular momentum $\mathbf{J}$). Electron states with different spin projection signs on $\mathbf{\Omega}(\mathbf{k})$ are split in energy, analogous to the Zeeman splitting in an external magnetic field. In zinc-blende crystals such as GaAs there is a cubic Dresselhaus term[12] $\mathbf{\Omega}_D \propto k^3$, whereas strain introduces a term $\mathbf{\Omega}_\varepsilon = C\Delta\varepsilon(k_x, -k_y, 0)$ that is linear in k, where $\Delta\varepsilon$ is the difference between strain in the $\hat{z}$ and $\hat{x},\hat{y}$ directions[13]. In wurtzite crystals or in multilayered materials with structural inversion asymmetry, there also exists the Rashba term[14] $\mathbf{\Omega}_R$, which has a different symmetry with respect to the direction of k, $\mathbf{\Omega}_R = \alpha_R(-k_y, k_x, 0)$, where $\hat{z}$ is along the axis of reduced symmetry. In the presence of an electric field, the electrons acquire an average momentum $\hbar\Delta\mathbf{k}(\mathbf{E})$, which leads to the generation of an electric current $\mathbf{j} = \hat{\rho}^{-1}\mathbf{E}$ in the conductor, where $\hat{\rho}$ is the resistivity tensor. This current defines the preferential axis for spin precession $\langle\Omega(\mathbf{j})\rangle$. As a result, a non-equilibrium current-induced spin polarization $\langle\mathbf{J}^E\rangle \| \langle\mathbf{\Omega}(\mathbf{j})\rangle$ is generated, the magnitude of which $\langle J^E\rangle$ depends on the strength of various mechanisms of momentum scattering and spin relaxation[5,15]. This spin polarization has been measured in non-magnetic semiconductors using optical[7–9,11,16] and electron spin resonance[17] techniques. It is convenient to parameterize $\langle\mathbf{J}^E\rangle$ in terms of an effective magnetic field $\mathbf{H}^{so}$. Different contributions to $\mathbf{H}^{so}$ have different current dependencies ($\propto j$ or j^3), as well as different symmetries with respect to the direction of $\mathbf{j}$, as schematically shown in Fig. 1c,d, enabling one to distinguish between spin polarizations in different fields.

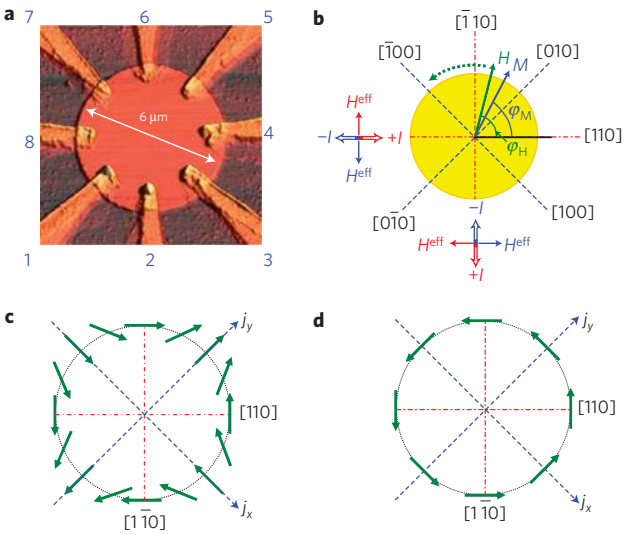

Figure 1 | Layout of the device and symmetry of the spin–orbit fields. **a**, Atomic force micrograph of sample A with eight non-magnetic metal contacts. **b**, Diagram of device orientation with respect to crystallographic axes, with easy and hard magnetization axes marked with blue dashed and red dot-dash lines, respectively. Measured directions of $\mathbf{H}^{eff}$ field are shown for different current directions. **c**,**d**, Orientation of effective magnetic field with respect to current direction for strain-induced (**c**) and Rashba (**d**) spin–orbit interactions. The current-induced Oersted field under the contacts has the same symmetry as the Rashba field.

To investigate interactions between the spin–orbit-generated magnetic field and magnetic domains, we have chosen (Ga,Mn)As, a p-type ferromagnetic semiconductor[18,19] with zinc-blende crystalline structure similar to GaAs. Ferromagnetic interactions in this material are carrier-mediated[20,21]. The total angular momentum of the holes $\mathbf{J}$ couples to the magnetic moment $\mathbf{F}$ of Mn ions by means

[1]Department of Physics and Birck Nanotechnology Center, Purdue University, West Lafayette, Indiana 47907, USA, [2]Department of Physics, University of Notre Dame, Notre Dame, Indiana 46556, USA. *These authors contributed equally to this work. †e-mail: leonid@purdue.edu.

of antiferromagnetic exchange $\mathcal{H}_{ex} = -A\mathbf{F}\cdot\mathbf{J}$. This interaction leads to the ferromagnetic alignment of magnetic moments of Mn ions and equilibrium polarization of hole spins. If further, non-equilibrium spin polarization of the holes $\langle\mathbf{J}^{E}\rangle$ is induced, the interaction of the hole spins with magnetic moments of Mn ions enables one to control ferromagnetism by manipulating $\mathbf{J}$. Magnetic properties of (Ga,Mn)As are thus tightly related to the electronic properties of GaAs. For example, strain-induced spin anisotropy of the hole energy dispersion is largely responsible for the magnetic anisotropy in this material. (Ga,Mn)As, epitaxially grown on the (001) surface of GaAs, is compressively strained, which results in magnetization $\mathbf{M}$ lying in the plane of the layer perpendicular to the growth direction, with two easy axes along the [100] and [010] crystallographic directions[22,23]. Recently, control of magnetization by means of strain modulation has been demonstrated[24]. In this letter, we use spin–orbit-generated polarization $\langle\mathbf{J}^{E}\rangle$ to manipulate ferromagnetism.

We report measurements on two samples fabricated from (Ga,Mn)As wafers with different Mn concentrations. The devices were patterned into circular islands with eight non-magnetic ohmic contacts, as shown in Fig. 1a and discussed in the Methods section. In the presence of a strong external magnetic field $\mathbf{H}$, the magnetization of the ferromagnetic island is aligned with the field. For weak fields, however, the direction of magnetization is primarily determined by magnetic anisotropy. As a small field ($5 < H < 20$ mT) is rotated in the plane of the sample, the magnetization is re-aligned along the easy axis closest to the field direction. Such rotation of magnetization by an external field is demonstrated in Fig. 2. For the current $\mathbf{I}\|[1\bar{1}0]$, the measured R_{xy} is positive for $\mathbf{M}\|[100]$ and negative for $\mathbf{M}\|[010]$. Note that R_{xy}, and thus also the magnetization, switches direction when the direction of $\mathbf{H}$ is close to the hard axes [110] and $[1\bar{1}0]$, confirming the cubic magnetic anisotropy of our samples. The switching angles $\varphi_H = \angle\mathbf{HI}$ where R_{xy} changes sign are denoted as $\varphi_H^{(i)}$ on the plot.

In the presence of both external and spin–orbit fields, we expect to see a combined effect of $\mathbf{H}^{so} + \mathbf{H}$ on the direction of magnetization. For small currents (a few microamperes) $H^{so} \approx 0$, and R_{xy} does not depend on the sign or the direction of the current. At large d.c. currents, the value of $\varphi_H^{(i)}$ becomes current dependent and we define $\Delta\varphi_H^{(i)}(I) = \varphi_H^{(i)}(I) - \varphi_H^{(i)}(-I)$. Specifically, for $\mathbf{I}\|[1\bar{1}0]$, the switching of magnetization $[010] \rightarrow [\bar{1}00]$ occurs for $I = +0.7$ mA at smaller $\varphi_H^{(1)}$ than for $I = -0.7$ mA, $\Delta\varphi_H^{(1)} < 0$. For $[0\bar{1}0] \rightarrow [100]$ magnetization switching, the I dependence of the switching angle is reversed, $\Delta\varphi_H^{(3)} > 0$. There is no measurable difference in switching angle for the $[\bar{1}00] \rightarrow [0\bar{1}0]$ and $[100] \rightarrow [010]$ transitions ($\Delta\varphi_H^{(2,4)} \approx 0$). When the current is rotated by 90° ($\mathbf{I}\|[110]$), we observe $\Delta\varphi_H^{(2)} > 0$, $\Delta\varphi_H^{(4)} < 0$ and $\Delta\varphi_H^{(1,3)} \approx 0$. Figure 2c shows that $\Delta\varphi_H^{(2)}(I)$ decreases as current decreases and drops below experimental resolution of 0.5° at $I < 50$ μA. Similar data are obtained for sample B (see Supplementary Fig. S4).

The data can be qualitatively understood if we consider an extra current-induced effective magnetic field $\mathbf{H}^{eff}$, as shown schematically in Fig. 1b. When an external field $\mathbf{H}$ aligns the magnetization along one of the hard axes, a small perpendicular field can initiate magnetization switching. For $\mathbf{I}\|[110]$, the effective field $\mathbf{H}^{eff}\|[\bar{1}10]$ aids the $[100] \rightarrow [010]$ magnetization switching, whereas it hinders the $[\bar{1}00] \rightarrow [0\bar{1}0]$ switching. For $\varphi_H^{(1)} \approx 90°$ and $\varphi_H^{(3)} \approx 270°$, where $[010] \rightarrow [\bar{1}00]$ and $[0\bar{1}0] \rightarrow [100]$ magnetization transitions occur, $\mathbf{H}^{eff}\|\mathbf{H}$ does not affect the transition angle, $\Delta\varphi_H^{(2,4)} = 0$. For $\mathbf{I}\|[1\bar{1}0]$, the direction of the field $\mathbf{H}^{eff}\|[110]$ is reversed relative to the direction of the current, compared with the $\mathbf{I}\|[110]$ case. The symmetry of the measured $\mathbf{H}^{eff}$ with respect to $\mathbf{I}$ coincides with the unique symmetry of the strain-related spin–orbit field (Fig. 1c).

The dependence of $\Delta\varphi_H^{(i)}$ on various magnetic fields and current orientations is summarized in Fig. 3a,b. Assuming that the angle of

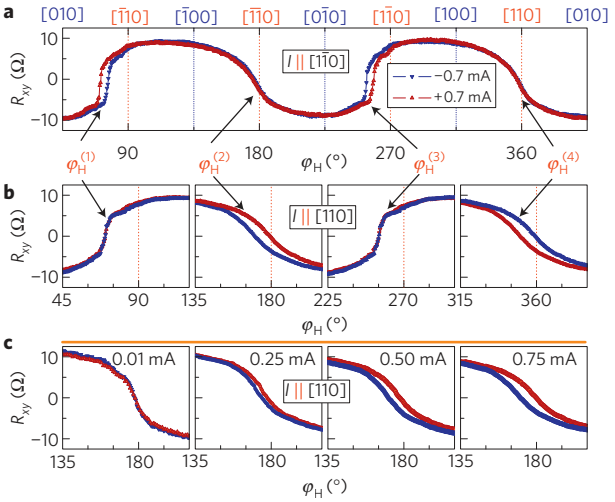

Figure 2 | Dependence of transverse anisotropic magnetoresistance on current and field orientation. a,**b**, Transverse anisotropic magnetoresistance R_{xy} as a function of external field direction φ_H for $H = 10$ mT and current $I = \pm 0.7$ mA in sample A. The angles $\varphi_H^{(i)}$ mark magnetization switchings. **c**, Magnetization switching between $[\bar{1}00]$ and $[0\bar{1}0]$ easy axes for several values of the current.

magnetization switching depends only on the total field $\mathbf{H}^{eff} + \mathbf{H}$, we can extract the magnitude H^{eff} and angle $\theta = \angle\mathbf{IH}^{eff}$ from the measured $\Delta\varphi_H^{(i)}$, thus reconstructing the whole vector $\mathbf{H}^{eff}$. Following a geometrical construction shown in Fig. 3d and taking into account that $\Delta\varphi_H^{(i)}$ is small, we find that

$$H^{eff} \approx H\sin(\Delta\varphi_H^{(i)}/2)/\sin(\theta - \varphi_H^{(i)})$$

and θ can be found from the comparison of switching at two angles. We find that $\theta \approx 90°$, or $\mathbf{H}^{eff} \perp \mathbf{I}$ for $I\|[110]$ and $I\|[1\bar{1}0]$. To further test our procedure, we carried out similar experiments with small current $I = 10$ μA but constant extra magnetic field $\delta\mathbf{H} \perp \mathbf{I}$ having the role of $\mathbf{H}^{eff}$. The measured $\delta H(\Delta\varphi_H)$ coincides with the applied δH within the precision of our measurements. (See Supplementary Fig. S5.)

In Fig. 3c, H^{eff} is plotted as a function of the average current density $\langle j\rangle$ for both samples. There is a small difference in the H^{eff} versus $\langle j\rangle$ dependence for $\mathbf{I}\|[110]$ and $\mathbf{I}\|[1\bar{1}0]$. The difference can be explained by considering the current-induced Oersted field $H^{Oe} \propto I$ in the metal contacts. The Oersted field is localized under the pads, which constitutes only 7% (2.5%) of the total area for sample A (B). The Oersted field has the symmetry of the field shown in Fig. 1d, and is added to or subtracted from the spin–orbit field, depending on the current direction. Thus, $H^{eff} = H^{so} + H^{Oe}$ for $\mathbf{I}\|[110]$ and $H^{eff} = H^{so} - H^{Oe}$ for $\mathbf{I}\|[1\bar{1}0]$. We estimate the fields to be as high as 0.6 mT under the contacts at $I = 1$ mA, which corresponds to $H^{Oe} \approx 0.04$ mT (0.015 mT) averaged over the sample area for sample A (B). These estimates are reasonably consistent with the measured values of 0.07 mT (0.03 mT). Finally, we determine H^{so} as an average of H^{eff} between the two current directions. The spin–orbit field depends linearly on j, as expected for strain-related spin–orbit interactions: $dH^{so}/dj = 0.53 \times 10^{-9}$ and 0.23×10^{-9} T cm^2 A^{-1} for samples A and B respectively.

We now compare the experimentally measured H^{so} with theoretically calculated effective spin–orbit field. In (Ga,Mn)As, the only term allowed by symmetry that generates H^{so} linear in the electric current is the Ω_ε term, which results in the directional dependence of $\mathbf{H}^{so}$ on $\mathbf{j}$ precisely as observed in

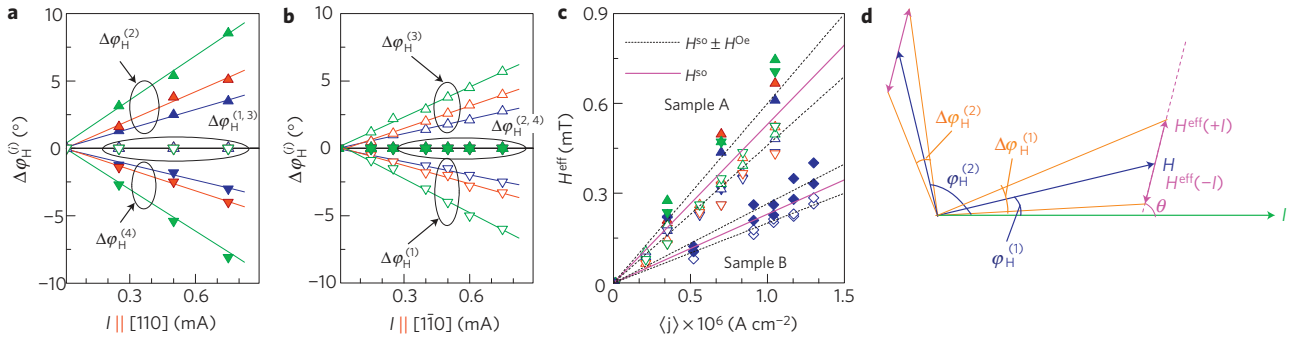

Figure 3 | Determination of current-induced effective spin–orbit magnetic field. a,**b**, Difference in switching angles for opposite current directions $\Delta\varphi_H^{(i)}$ as a function of I for sample A for different external fields H for orthogonal current directions. **c**, The measured effective field $H^{eff} = H^{so} \pm H^{Oe}$ as a function of average current density $\langle j \rangle$ for sample A (triangles) and sample B (diamonds). **d**, Schematic diagram of the different angles involved in determining H^{eff}: φ_H is the angle between current **I** and external magnetic field **H**; $\Delta\varphi_H$ is the angle between total fields $\mathbf{H}+\mathbf{H}^{eff}(+I)$ and $\mathbf{H}+\mathbf{H}^{eff}(-I)$ and θ is the angle between **I** and $\mathbf{H}^{eff}(+I)$.

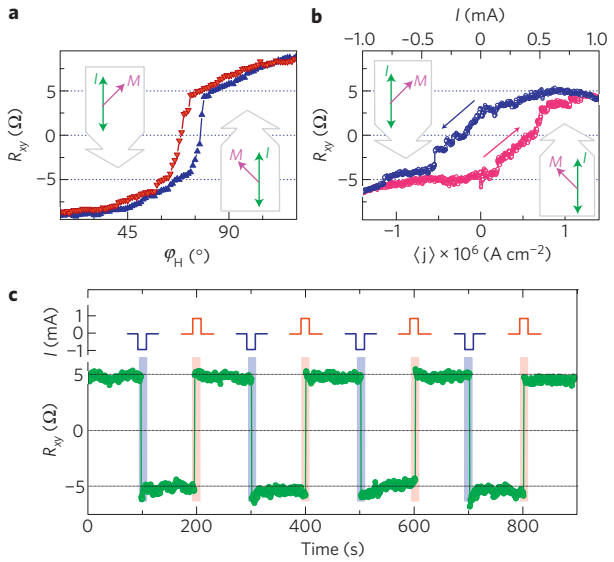

Figure 4 | Current-induced reversible magnetization switching. a, φ_H dependence of R_{xy} near the [010] → [$\bar{1}$00] magnetization switching for $I = \pm 0.7$ mA in sample A for $I \| [1\bar{1}0]$. **b**, R_{xy} shows hysteresis as a function of current for a fixed field $H = 6$ mT applied at $\varphi_H = 72°$. **c**, Magnetization switches between the [010] and [$\bar{1}$00] directions when alternating ±1.0 mA current pulses are applied. The pulses have 100 ms duration and are shown schematically above the data curve. R_{xy} is measured with $I = 10$ μA.

experiment. As for the magnitude of H^{so}, for three-dimensional $J = 3/2$ holes we obtain

$$\mathbf{H}^{so}(\mathbf{E}) = \frac{eC\Delta\varepsilon}{g^*\mu_B}\frac{(-38n_h\tau_h + 18n_l\tau_l)}{217(n_h+n_l)}\cdot(E_x, -E_y, 0)$$

where **E** is the electric field, g^* is the Luttinger Landé factor for holes, μ_B is the Bohr magneton and $n_{h,l}$ and $\tau_{h,l}$ are densities and lifetimes for the heavy (h) and light (l) holes. Detailed derivation of H^{so} is given in the Supplementary Information. Using this result, we estimate $dH^{so}/dj = 0.6 \times 10^{-9}$ T cm^2 A^{-1} assuming $n_h = n \gg n_l$ and $\tau_h = m_h/(e^2\rho n)$, where ρ is the resistivity measured experimentally, and using $\Delta\varepsilon = 10^{-3}$, $n = 2 \times 10^{20}$ cm^{-3}. The agreement between theory and experiment is excellent. It is important to note, however, that we used GaAs band parameters[25] $m_h = 0.4\,m_0$, where m_0 is the free electron mass, $g^* = 1.2$ and $C = 2.1$ eV Å. Although the corresponding parameters for (Ga,Mn)As are not known, the use of GaAs parameters seems reasonable. We note, for example, that GaAs parameters adequately described tunnelling anisotropic magnetoresistance in recent experiments[26].

Finally, we demonstrate that the current-induced effective spin–orbit field H^{so} is sufficient to reversibly manipulate the direction of magnetization. Figure 4a shows the φ_H dependence of R_{xy} for sample A, showing the [010] → [$\bar{1}$00] magnetization switching. If we fix $H = 6$ mT at $\varphi_H = 72°$, R_{xy} forms a hysteresis loop as current is swept between ±1 mA. R_{xy} is changing between ±5 Ω, indicating that **M** is switching between the [010] and [$\bar{1}$00] directions. Short (100 ms) 1 mA current pulses of alternating polarity are sufficient to permanently rotate the direction of magnetization. The device thus performs as a non-volatile memory cell, with two states encoded in the magnetization direction, the direction being controlled by the unpolarized current passing through the device. The device can be potentially operated as a four-state memory cell if both the [110] and [$\bar{1}$10] directions can be used to inject current. We find that we can reversibly switch the magnetization with currents as low as 0.5 mA (current densities 7×10^5 A cm^{-2}), an order of magnitude smaller than by polarized current injection in ferromagnetic metals[1–3], and just a few times larger than by externally polarized current injection in ferromagnetic semiconductors[4].

Methods

The (Ga,Mn)As wafers were grown by molecular beam epitaxy at 265 °C and subsequently annealed at 280 °C for 1 h in nitrogen atmosphere. Sample A was fabricated from a 15-nm-thick epilayer with 6% Mn, and sample B from a 10-nm-thick epilayer with 7% Mn. Both wafers have a Curie temperature $T_c \approx 80$ K. The devices were patterned into 6- and 10-μm-diameter circular islands to decrease domain pinning. Cr/Zn/Au (5 nm/10 nm/300 nm) ohmic contacts were thermally evaporated. All measurements were carried out in a variable-temperature cryostat at $T = 40$ K for sample A and at 25 K for sample B, well below the temperature of (Ga,Mn)As-specific cubic-to-uniaxial magnetic anisotropy transitions[27], which has been measured to be 60 and 50 K for the two wafers. The temperature rise for the largest currents used in the reported experiments was measured to be <3 K.

Transverse anisotropic magnetoresistance $R_{xy} = V_y/I_x$ is measured using the four-probe technique, which ensures that possible interfacial resistances, for example, those related to the antiferromagnetic ordering in the Cr wetting layer[28], do not contribute to the measured R_{xy}. The d.c. current I_x was applied either along the [110] (contacts 4–8 in Fig. 1a) or along the [1$\bar{1}$0] (contacts 2–6) direction. Transverse voltage was measured in the Hall configuration, for example, between contacts 2–6 for $I_x \| [110]$. To ensure uniform magnetization of the island, magnetic field was ramped to 0.5 T after adjusting the current at the beginning of each field rotation scan. We monitor V_x between different contact sets (for example, 1–7, 4–6 and 3–5) to confirm the uniformity of magnetization within the island.

To determine the direction of magnetization **M**, we use the dependence of R_{xy} on magnetization[29]:

$$R_{xy} = \Delta\rho \sin\varphi_M \cos\varphi_M$$

where $\Delta\rho = \rho_\| - \rho_\perp$, $\rho_\| < \rho_\perp$ are the resistivities for magnetization oriented parallel and perpendicular to the current, and $\varphi_M = \angle\mathbf{MI}$ is an angle between magnetization and current. In a circular sample, the current distribution is

non-uniform and the angle between the magnetization and the local current density varies throughout the sample. However, the resulting transverse anisotropic magnetoresistance depends only on φ_M. For the current-to-current-density conversion, we model our sample as a perfect disc with two point contacts across the diameter. The average current density in the direction of current injection is $\langle j \rangle = 2I/(\pi ad)$, where a is the disc radius and d is the (Ga,Mn)As layer thickness. In a real sample, the length of contact overlap with (Ga,Mn)As ensures that j changes by less than a factor of 3 throughout the sample. A detailed discussion of the current distribution and of measurements of joule heating can be found in the Supplementary Information.

Received 17 December 2008; accepted 2 July 2009; published online 2 August 2009

References

1. Slonczewski, J. C. Current-driven excitation of magnetic multilayers. *J. Magn. Magn. Mater.* **159,** 1–7 (1996).
2. Berger, L. Emission of spin waves by a magnetic multilayer traversed by a current. *Phys. Rev. B* **54,** 9353–9358 (1996).
3. Myers, E. B., Ralph, D. C., Katine, J. A., Louie, R. N. & Buhrman, R. A. Current-induced switching of domains in magnetic multilayer devices. *Science* **285,** 867–870 (1999).
4. Chiba, D., Sato, Y., Kita, T., Matsukura, F. & Ohno, H. Current-driven magnetization reversal in a ferromagnetic semiconductor (Ga,Mn)As/GaAs/(Ga,Mn)As tunnel junction. *Phys. Rev. Lett.* **93,** 216602 (2004).
5. Aronov, A. G. & Lyanda-Geller, Y. B. Nuclear electric resonance and orientation of carrier spins by an electric field. *JETP Lett.* **50,** 431–434 (1989).
6. Edelstein, V. M. Spin polarization of conduction electrons induced by electric current in two-dimensional asymmetric electron systems. *Solid State Commun.* **73,** 233–235 (1990).
7. Kalevich, V. K. & Korenev, V. L. Effect of electric field on the optical orientation of 2d electrons. *JETP Lett.* **52,** 230–235 (1990).
8. Kato, Y., Myers, R. C., Gossard, A. C. & Awschalom, D. D. Coherent spin manipulation without magnetic fields in strained semiconductors. *Nature* **427,** 50–53 (2004).
9. Silov, A. Y. *et al.* Current-induced spin polarization at a single heterojunction. *Appl. Phys. Lett.* **85,** 5929–5931 (2004).
10. Ganichev, S. D. Spin-galvanic effect and spin orientation by current in non-magnetic semiconductors. *Int. J. Mod. Phys. B* **22,** 1–26 (2008).
11. Meier, L. *et al.* Measurement of Rashba and Dresselhaus spin–orbit magnetic fields. *Nature Phys.* **3,** 650–654 (2007).
12. Dresselhaus, G. Spin–orbit coupling effects in zinc blende structures. *Phys. Rev.* **100,** 580–586 (1955).
13. Bir, G. L. & Pikus, G. E. *Symmetry and Strain-Induced Effects in Semiconductors* (Wiley, 1974).
14. Bychkov, Y. A. & Rashba, E. I. Oscillatory effects and the magnetic susceptibility of carriers in inversion layers. *J. Phys. C: Solid State Phys.* **17,** 6039–6045 (1984).
15. Aronov, A. G., Lyanda-Geller, Y. B. & Pikus, G. E. Spin polarization of electrons by an electric current. *Sov. Phys. JETP* **73,** 537–541 (1991).
16. Golub, L. E. *et al.* Electric current-induced spin orientation in quantum well structures. *J. Magn. Magn. Mater.* **300,** 127–131 (2006).
17. Wilamowski, Z., Malissa, H., Schaffler, F. & Jantsch, W. g-factor tuning and manipulation of spins by an electric current. *Phys. Rev. Lett.* **98,** 187203 (2007).
18. Ohno, H. *et al.* (Ga,Mn)As: A new diluted magnetic semiconductor based on GaAs. *Appl. Phys. Lett.* **69,** 363–365 (1996).
19. Ohno, H. Making nonmagnetic semiconductors ferromagnetic. *Science* **281,** 951–956 (1998).
20. Dietl, T., Ohno, H., Matsukura, F., Cibert, J. & Ferrand, D. Zener model description of ferromagnetism in zinc-blende magnetic semiconductors. *Science* **287,** 1019–1022 (2000).
21. Berciu, M. & Bhatt, R. N. Effects of disorder on ferromagnetism in diluted magnetic semiconductors. *Phys. Rev. Lett.* **87,** 107203 (2001).
22. Welp, U., Vlasko-Vlasov, V. K., Liu, X., Furdyna, J. K. & Wojtowicz, T. Magnetic domain structure and magnetic anisotropy in $Ga_{1-x}Mn_xAs$. *Phys. Rev. Lett.* **90,** 167206 (2003).
23. Liu, X., Sasaki, Y. & Furdyna, J. K. Ferromagnetic resonance in $Ga_{1-x}Mn_xAs$: Effects of magnetic anisotropy. *Phys. Rev. B* **67,** 205204 (2003).
24. Overby, M., Chernyshov, A., Rokhinson, L. P., Liu, X. & Furdyna, J. K. GaMnAs-based hybrid multiferroic memory device. *Appl. Phys. Lett.* **92,** 192501 (2008).
25. Chantis, A. N. *et al.* Strain-induced conduction-band spin splitting in GaAs from first-principles calculations. *Phys. Rev. B* **78,** 075208 (2008).
26. Elsen, M. *et al.* Exchange-mediated anisotropy of (Ga,Mn)As valence-band probed by resonant tunneling spectroscopy. *Phys. Rev. Lett.* **99,** 127203 (2007).
27. Chiba, D. *et al.* Magnetization vector manipulation by electric fields. *Nature* **455,** 515–518 (2008).
28. Smit, P. & Alberts, H. L. On magnetic transitions in dilute Cr–Ga and Cr–Ge alloys. *J. Appl. Phys.* **63,** 3609–3610 (1988).
29. Tang, H. X., Kawakami, R. K., Awschalom, D. D. & Roukes, M. L. Giant planar Hall effect in epitaxial (Ga,Mn)As devices. *Phys. Rev. Lett.* **90,** 107201 (2003).

Acknowledgements

This work was supported in part by NSF under the grants ECS-0348289 (L.P.R.) and DMR-0603752 (J.K.F.).

Author contributions

A.C. and M.O. fabricated samples and carried out measurements, X.L. and J.K.F. designed and grew (Ga,Mn)As wafers specifically for these experiments, Y.L.-G. developed the theory and L.P.R. designed and supervised the experiments.

Additional information

Supplementary information accompanies this paper on www.nature.com/naturephysics. Reprints and permissions information is available online at http://npg.nature.com/reprintsandpermissions. Correspondence and requests for materials should be addressed to L.P.R.

nature physics

SUPPLEMENTARY INFORMATION

DOI: 10.1038/NPHYS1362

Evidence for the reversible control of magnetization in a ferromagnetic material via spin-orbit magnetic field

A. Chernyshov, M. Overby, X. Liu, J. K. Furdyna, Y. Lyanda-Geller, and L. P. Rokhinson

I. JOULE HEATING

(Ga,Mn)As is a magnetic semiconductor with strong temperature dependence of resistivity, see Fig. S1(a). The enhancement of resistivity at 80 K is due to the enhancement of spin scattering in the vicinity of the Curie temperature T_C. Inelastic scattering length in these materials is just a few tenths of nm, and we expect holes to be in thermal equilibrium with the lattice[1]. Thus resistivity can be used to measure the temperature of the sample.

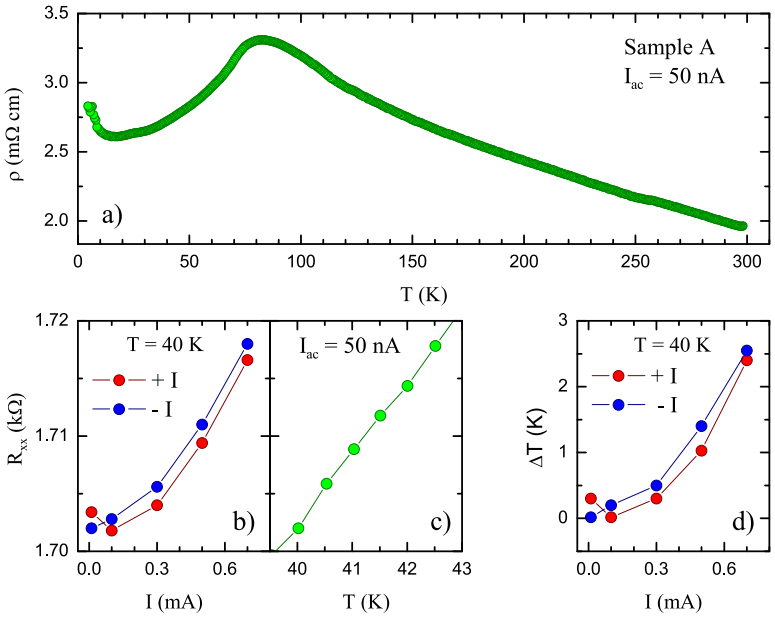

FIG. S1: **Current-induced heating** a) Temperature dependence of resistivity for sample A; b) current and c) temperature dependence of sample resistance in the vicinity of 40 K; d) sample heating as a function of dc current.

In Fig. S1(b,c) we plot temperature and current dependences of the sample resistance in the vicinity of 40 K. This data is combined in (d), where the sample temperature change ΔT due to Joule heating is plotted as a function of dc current. The maximum temperature rise does not exceed 3 K at $I = 0.7$ mA in our experiments. This small heating ensures that the sample temperature stays well below the Curie temperature ($\approx$ 80 K) and the (Ga,Mn)-specific cubic-to-uniaxial magnetic anisotropy transition ($\approx$ 60 K for sample A and $\approx$ 50 K for sample B) when experiments are performed at 40 K and 25 K for samples A and B, respectively. Observation of different angles for magnetization switching for $+I$ and $-I$ (Fig. 2) further confirms that heating is not responsible for the reported effects (Joule heating is $\propto J^2$ and does not depend on the current direction).

II. CURRENT DISTRIBUTION IN CIRCULAR SAMPLES

Magnetization-dependent scattering in (Ga,Mn)As results in an anisotropic correction to the resistivity tensor $\hat{\rho}$ which depends on the angle φ_m between magnetization $\mathbf{M}$ and local current density $\mathbf{j}$ [2]:

$$\begin{aligned} \rho_{xx} &= \rho_\perp + (\rho_\parallel - \rho_\perp)\cos^2(\varphi_m), \\ \rho_{xy} &= (\rho_\parallel - \rho_\perp)\sin(\varphi_m)\cos(\varphi_m), \end{aligned} \tag{S1}$$

DOI: 10.1038/NPHYS1362

where $\rho_{||}$ ($\rho_{\perp}$) are the resistivities for $\mathbf{j}||\mathbf{M}$ ($\mathbf{j}\perp\mathbf{M}$), and we assumed that both $\mathbf{j}$ and $\mathbf{M}$ lie within the plane of the sample. The off-diagonal resistivity (transverse anisotropic magnetoresistance) ρ_{xy} can be non-zero even in the absence of the external magnetic field. The difference $(\rho_{||}-\rho_{\perp})/\rho_{\perp} \approx 0.01$ and we first calculate the local potential $\phi_0(x,y)$ inside the sample by approximating it as a disk of radius a and thickness d with isotropic resistivity $\rho_0 = (\rho_{\parallel}+\rho_{\perp})/2$:

$$\phi_0 = \frac{\rho_0 I}{\pi d}\ln\left[\frac{(a-x)^2+y^2}{(a+x)^2+y^2}\right], \tag{S2}$$

where current I is injected along the $\hat{x}$-axis. Current density $\mathbf{j} = \nabla\phi_0/\rho_0$ is plotted in Fig. S2(a). Metal contacts have a radius of ≈ 0.5 μm in our samples, which limits the current density near the current injection regions. Integrating j over the sample area we find average current density

$$\langle j_x\rangle = \frac{2I}{\pi a d},\ \langle j_y\rangle = 0. \tag{S3}$$

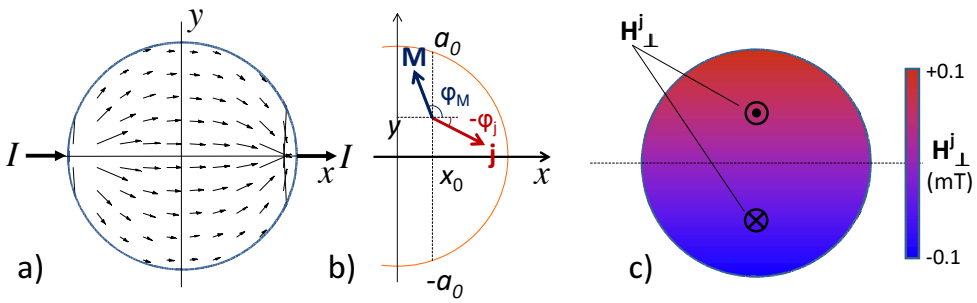

FIG. S2: **Current distribution** a) Vector plot of local current density $\mathbf{j}(x,y)$ distribution in the sample; b) angles between $\mathbf{j}(x,y)$, magnetization $\mathbf{M}$ and current $\mathbf{I}\|\hat{x}$ are defined; c) Color map plot of Oersted field ($H_{\perp}^{j}$) distribution in a disk-shaped sample.

We find the transverse voltage V_y as a correction to the ϕ_0 potential due to the anisotropic resistivity $\rho_{||}-\rho_{\perp} \neq 0$:

$$V_y(x_0) = \int_{-a_0}^{a_0}\left[-\rho_{xy}\cdot j_x(y) + \rho_{xx}\cdot j_y(y)\right]dy. \tag{S4}$$

The current distribution is non-uniform, and the local electric field depends on the total angle $\varphi_m = \varphi_M - \varphi_j$, where $\varphi_M = \widehat{\mathbf{MI}}$ and $\varphi_j = \widehat{\mathbf{jI}}$, see Fig. S2(b). This integral can be evaluated analytically, and the transverse anisotropic magnetoresistance (AMR) R_{xy} is found to be the same as for an isotropic current flow, independent of the distance x_0 of the voltage contacts from the center of the disk:

$$R_{xy} = V_y/I = (\rho_{||}-\rho_{\perp})\cos(\varphi_M)\sin(\varphi_M). \tag{S5}$$

The magnetization angle φ_M can therefore be directly calculated from the measured transverse resistance R_{xy}.

III. CURRENT-GENERATED OERSTED MAGNETIC FIELDS

In this section we estimate conventional current-generate magnetic fields in our device that are not related to spin-orbit interactions. There are two contributions to the Oersted magnetic fields: a magnetic field due to non-uniform current distribution within the sample, and a field generated by high currents in the vicinity of the metal contacts.

We can calculate the Oersted field inside (Ga,Mn)As by using the Biot-Savart formula:

$$\mathbf{H} = \frac{\mu_0}{4\pi}\int\frac{\mathbf{j}\times\hat{\mathbf{r}}}{r^2}dV, \tag{S6}$$

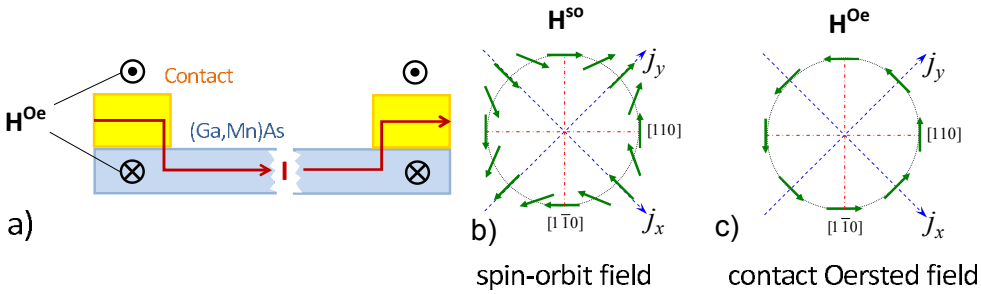

FIG. S3: **Oersted field** a) schematic illustration of the origin of the in-plane Oersted field H^{Oe} under gold contact pads; b,c) symmetry of H^{so} and H^{Oe} fields.

where μ_0 is the permeability of free space, and the integral is taken over the volume of the disk. The most significant $H_\perp^j$ normal component of the field is shown in Fig. S2(c). The largest $H_\perp^j \leq 1$ Oe, which is negligible compared to the 2000 Oe anisotropy field that keeps the magnetization in-plane.

The second contribution to the Oersted field originates from contact pads, see Fig. S3. The conductivity of gold contacts is much higher that of (Ga,Mn)As, and the current flows predominantly through the metal within contact regions, thus generating both in-plane ($H_\parallel^{Oe}$) and out-of plane ($H_\perp^{Oe}$) magnetic fields in (Ga,Mn)As underneath and at the edges of the contact pads. The maximum value of the field can be estimated as $H_\perp^{Oe} \approx H_{||}^{Oe} = \mu_0 I/2w$, where I is the total current and $w = 1$ μm is the width of the contact pad. This field can be as high as 6 Oe for $I = 1$ mA. The field is localized under the pads, which constitute only 1/12th of the sample area.

The $H_\perp^{Oe}$ field does not induce in-plane magnetization rotation. The $H_\parallel^{Oe}$ field and the effective spin-orbit field have different symmetries with respect to the current rotation, see Fig. S2(b,c), and thus can be experimentally distinguished. The two fields point in the same direction for $\mathbf{I}||[110]$, but in the opposite direction for the current rotated by 90°, $\mathbf{I}||[1\bar{1}0]$. Experimentally, we observe an effective field which corresponds to the symmetry of the SO effective field. However, there is a small difference in the slopes of $\Delta\phi_H$ vs I curves for the two orthogonal current directions, Fig. 3(a,b), because the contact field is added to the SO field for $\mathbf{I}||[110]$ and subtracted from SO field for $\mathbf{I}||[1\bar{1}0]$. Both fields $\propto I$. From the ratio of the slopes (≈ 1.2) we can calculate the strength of the contact field, $H_\perp^{Oe} \approx 0.1 H^{so}$. This experimentally found ratio is consistent with the above estimate if we average the contact Oersted field over the sample area.

IV. DEPENDENCE OF TRANSVERSE ANISOTROPIC MAGNETORESISTANCE ON CURRENT AND FIELD ORIENTATION

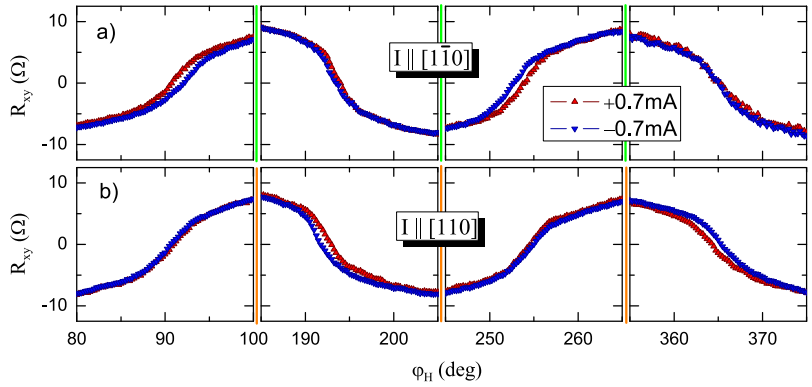

FIG. S4: **Dependence of transverse anisotropic magnetoresistance on current and field orientation for Sample B.** Transverse anisotropic magnetoresistance R_{xy} is plotted for current $\mathbf{I}||[1\bar{1}0]$ (a) and $\mathbf{I}||[110]$ (b) for $I = \pm 0.75$ mA with constant magnetic field $H = 20$ mT as a function of field angle φ_H.

In order to test the procedure of the effective field mapping, we performed control experiments where a small

DOI: 10.1038/NPHYS1362

constant external magnetic field $\delta\mathbf{H}\perp\mathbf{I}$ was playing the role of spin-orbit field. In these experiments the current was reduced to $I = 10$ μA. The results, shown in Fig. S5, are quantitatively similar to the effect of the spin-orbit field.

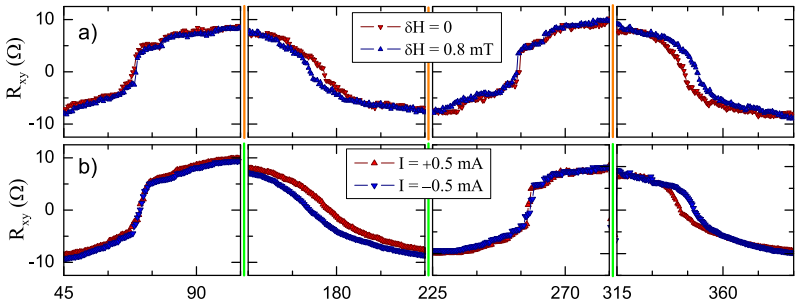

FIG. S5: **Control experiment with additional external field** a) R_{xy} is plotted for Sample A with $\mathbf{H_{total}} = \delta\mathbf{H} + \mathbf{H}$, where $\delta H\perp\mathbf{I}$ and $I = 10$ μA, $\delta H = 0, 0.8$ mT. For comparison, in b) similar data are plotted for $\delta H = 0$ but $I = \pm 0.5$ mA.

V. CALCULATION OF THE EFFECTIVE SPIN-ORBIT FIELD INDUCED BY THE ELECTRIC CURRENT

Manipulation of localized spins, electronic, nuclear or ionic, can be achieved via manipulation of free carrier spins. The free carrier spins can be manipulated by the external magnetic field, by the Oersted magnetic field of the current, and by the electric current via intrinsic spin-orbit interactions. The intrinsic spin-orbit interactions arise in crystalline systems, in which axial vectors, such as spin polarization, and polar vectors, such as the electric current, behave equivalently with respect to the symmetry trasformations of a crystal. The crystal symmetry then allows the transformation of the electric current into a spin polarization of charge carriers. In this work, Mn ions of the ferromagnetic semiconductor (Ga,Mn)As, and thus its ferromagnetic properties, are affected by the electric current via the intrinsic spin-orbit interactions.

In (Ga,Mn)As, charge carriers are holes with an angular momentum $\mathbf{J} = 3/2$. In contrast to electron systems, the hole system is defined by a very strong coupling of the total angular momentum $\mathbf{J}$ to the hole momentum $\mathbf{p}$, which includes both terms quadratic in $\mathbf{p}$ and independent of $\mathbf{p}$. These terms are quadratic in $\mathbf{J}$, and they are not present for electrons with spin 1/2. The Luttinger-Pikus Hamiltonian quadratic in $\mathbf{J}$ is[3]

$$\mathcal{H}_h = A_0 p^2 + A_1 \sum_i J_i^2 p_i^2 + A_2 \sum_{i,j\neq i} J_i J_j p_i p_j + B_1 \sum_i \varepsilon_{ii} J_i^2 + B_2 \sum_{i,j\neq i} J_i J_j \varepsilon_{ij}, \tag{S7}$$

where $i, j = x, y, z$. Despite the presence of a very strong spin-orbit coupling, which leads to the spectral splitting of holes into two pairs of states, this Hamiltonian on its own cannot result in a spin polarization of holes induced by the electric current. Terms capable of generating spin polarization in systems characterized by the absence of center of symmetry in the crystal and by a corresponding additional lowering of the crystalline symmetry in the presence of strain, read

$$\mathcal{H}' = \gamma_v \sum_i J_i p_i (p_{i+1}^2 - p_{i+2}^2) + C \sum_i [J_i p_i (\varepsilon_{i+1,i+1} - \varepsilon_{i+2,i+2}) + (J_i p_{i+1} - J_{i+1} p_i)\varepsilon_{i,i+1}], \tag{S8}$$

where cyclic permutation of indices is implied. The first term is cubic in the hole momentum, and it can lead only to the polarization of hole spins cubic in the electric current (and only when the current direction is away from the high symmetry axes). For effects linear in electric current this term is only relevant insofar as it contributes to the spin relaxation of the holes. The third term contains off-diagonal components of the strain tensor, and is negligible in (Ga,Mn)As crystals under study. In this system, strain originates from doping by Mn ions, and constitutes tension along the growth axis $z||[001]$ defined by the component ε_{zz} and $\Delta\varepsilon = \varepsilon_{zz} - \varepsilon_{xx} = \varepsilon_{zz} - \varepsilon_{yy}$. Thus only the second term results in a current-induced spin polarization. The symmetry of the corresponding effective field, $\mathbf{\Omega}(\mathbf{p}) = C\Delta\varepsilon(p_x, -p_y, 0)$, depends markedly on the crystallographic orientation. When an electric field is applied, the direction of the generated hole spin polarization with respect to the orientation of the electric current is the same as

the direction of the SO effective field with respect to the hole momentum. Such peculiar symmetry differs from the symmetry of the Oersted magnetic field, and thus allows one to distinguish between these effects.

We consider now the approximation linear in strain, when only the strain-dependent term proportional to C is taken into account, and strain-dependent terms in $\mathcal{H}_h$ are omitted. In this case the hole spectrum given by $\mathcal{H}_h$ splits into heavy (h) and light (l) hole branches. The mechanism of generation a spin polarization by the effective SO field in the presence of an electric current is simply a shift in the distribution functions for heavy and light holes in momentum space. In contrast low symmetry electron systems[4], where spin polarization is associated entirely with the relaxation of spins, in case of holes the spin relaxation occurs on the time scale of momentum relaxation and plays no role in the current-induced spin polarization. At low temperatures the hole angular momentum density is given by

$$\langle J_i^{(\mathbf{E})} \rangle = (-1)^i \frac{eE_i C \Delta\varepsilon}{E_F} \Big(\frac{-38}{35} n_h \tau_h + \frac{18}{35} n_l \tau_l \Big), \tag{S9}$$

where $i = 1, 2$ correspond to principal axes x and y, characteristic times $\tau_{h,l}$ are defined by mobilities of holes in the corresponding bands, and $n_{h(l)}$ are densities of holes in these bands. At room temperatures E_F in the denominator is to be replaced by $3/2k_BT$, T being the lattice temperature and k_B the Boltzman constant. Estimates show that the negative term in brackets of Eq. S9 is dominant.

We note that in the case of very strong deformations the spin relaxation of holes occurs on the times scale longer than that of momentum relaxation. Then simple shift of hole distribution functions in momentum space is no longer sufficient for generating spin polarization by current, and the mechanism of the effect becomes analogous to that for electrons[4]. We will present the results for hole spin polarization generated by electric current at arbitrary value of strain elsewhere.

The spin polarization given by Eq. S9 leads to an effective magnetic field acting on the Mn ions. In order to calculate what external magnetic field would result in the same polarization as that generated by the current, we calculate the average spin density induced by an external magnetic field:

$$\langle J_i^{(\mathbf{H})} \rangle = \frac{31 g^* \mu_B H (n_h + n_l)}{5 E_F} \tag{S10}$$

The ratio of polarizations $\langle J_i^{(\mathbf{E})} \rangle$ and $\langle J_i^{(\mathbf{H})} \rangle$ gives the electric field polarization measured in units of magnetic field. We note that while the SO field affects Mn ions only via the exchange interaction, the Oersted or the external magnetic field also acts on the ions directly. However, the magnitude of the exchange interaction, $A = -5$ meV is quite large, making the exchange interaction dominant. We will therefore omit the discussion of direct polarization of Mn by external fields.

[1] L. P. Rokhinson *et al.*, *Weak Localization in $Ga_{1-x}Mn_xAs$: Evidence of Impurity Band Transport*, Phys. Rev. B **76**, 161201 (2007).
[2] H. X. Tang, R. K. Kawakami, D. D. Awschalom, and M. L. Roukes, *Giant planar Hall effect in epitaxial (Ga,Mn)As devices*, Phys. Rev. Lett. **90**, 107201 (2003).
[3] G. L. Bir and G. E. Pikus, *Symmetry and strain-induced effects in semiconductors* (Wiley, New York, 1974).
[4] A.G. Aronov, Yu.B. Lyanda-Geller, and G.E. Pikus, *Spin polarization of electrons by an electric current*, Sov. Phys. JETP **73**, 537 (1991).